Silicon
https://doi.org/10.1007/s12633-023-02477-5

RESEARCH

Newly Fabricated Ternary PAAm-PVA-PVP Blend Polymer Doped by SiO_2: Absorption and Dielectric Characteristics for Solar Cell Applications and Antibacterial Activity

Athar Iqbal Alawi[1,2] · **Ehssan Al-Bermany**[1]

Received: 4 March 2023 / Accepted: 18 April 2023

Abstract
Silicon oxide nanoparticles (SiO_2 NPs) attracted nanomaterials for tuning the structure, characterizations, band gap, and dielectric properties. Newly ternary blend polymers nanocomposites reinforced using SiO_2 nanoparticles were fabricated and investigated. Poly(acrylamide) (PAAm), poly(vinyl alcohol) (PVA), and poly(vinyl pyrrolidone) (PVP) were mixed with different ratios and loaded with different ratios of SiO_2 (x = 0.00, 0.01, 0.03, and 0.05) wt. % applying green-easy solution-casting procedure. X-ray diffraction (XRD), infrared Fourier-transform spectroscopy (FTIR), optical microscopy (OPM), field emission scanning electron microscope (FE-SEM), UV–visible spectrophotometer, DC electrical meter and antibacterial activity of the nanocomposite were used to characterizations the samples. FTIR spectra exhibited significant interfacial interaction between the component matrixes. XRD patterns for samples showed a broad peak between ~ 10–50°. OPM and FESEM images showed a homogeneous surface and excellent distribution of nanoparticles in the matrix. The optical absorption results enhanced from 0.73 to 0.91 at 200 nm, and the energy gap improved from 4.8 to 3.4 eV for allowed indirect transition and from 4.2 to 3.1 eV for forbidden indirect transition. The dielectric constant and loss improved from 0.20 to 0.53, and outstanding enhancement was presented in the electrical conductivity. SiO_2 NPs exhibited notable improvement in the inhibited zone of antibacterial activity from 0.00 to 24 mm of S. aureus and 23 mm of E. coli compared to ternary blend polymers. These nanocomposites are promising for various applications, such as solar cells, optoelectronic, and biology applications.

Keywords SiO_2 · PAAm · PVP · PVA · Absorption · Dialectical · Optoelectronic · Antibacterial · Nanocomposites

1 Introduction

The efficiency of polymer-based solar cells could be lower than silicon-based solar cells, which could relate to the lack of absorbing the whole solar light by the photoactive layer. The polymer with a large band gap presented emission quenching, which is a problem by presenting only one donor compared to the two acceptors in the ternary blend [1]. Therefore, many researchers tried solving this issue using binary blend counterparts. Other investigated using ternary blend polymers that showed better absorption optical range and can be easily expanded. This impact comes from additional absorption of the third material that can be more expeditiously get donor/acceptor interfaces through the transfer of the long-range energy [2]. Compared to binary blend counterparts, there is a significant enhancement to the photocurrent generation of ternary blend polymer solar cells [1, 2]. Recently, a ternary structure has been a promising strategy to enhance the performances in binary polymer, fullerene, and bulk heterojunction polymer (BHJ) devices [3]. To boost the achievement in the material properties, incorporating the nanostructures such as SiO_2, TiO_2, GO, and Ag nanoparticles in these ternary blends polymer can play a unique role in improving the emission of the large band gap polymer by a mechanism, which is named charge trapping [1].

Silicon is a promising material with significant characterizations because it has chemical stability, a high melting

✉ Ehssan Al-Bermany
ehssan@itnet.uobabylon.edu.iq

[1] Department of Physics, College of Education for Pure Science, University of Babylon, Babylon, Iraq

[2] Educational Directorate of Babylon, Ministry of Education, Baghdad, Iraq

Published online: 27 April 2023

point of (1700 °C), etc. These important features make silicon a primary dielectric in silicon electronic technology and a superb thermal and electrical insulator [4]. Additionally, most of the standard current of optical fiber communication is made from silicon [5]. The nanoparticles are created by first depositing a silicon-rich material, followed by heat treatments that cause the excess silicon to precipitate [5]. Silicon dioxide or silica is a silicon oxide with the most common in nature as quartz [2]. Silicon dioxide (SiO_2) is a usually diffused adsorbent resistant to high temperatures, low cost, and non-toxic material [6]. The development of mini bands and subsequent widening of the influential band gap result from reduced silicon particle diameter to the nanometric scale. In addition to crystalline silicon dioxide, modern electronics rely heavily on it to produce nanocomposite materials for semiconductors and microelectronic devices [5, 7]. These nanomaterials can benefit from both parts' advantageous traits to fabricate polymer-nanocomposite materials [8]. Nanoparticles have been reported that bring unique properties and notable improvements in structural-property relationships [9, 10] and are used in modern applications when reinforcing the polymer blend [11, 12]. Meanwhile, a blend of two or more polymers could achieve unique properties of hybrid/nanocomposite materials and open a wide range of required properties for specific or general applications [7, 13]. These blended polymers could achieve more benefits and enable more by loading with nanofillers [10]. The final qualities of polymer-nanocomposite materials could change by adjusting the component concentration within the composition of the polymeric matrix [8].

Polyacrylamide (PAAm) is unique as it does not resemble a monomer and is non-toxic due to the 19.7% nitrogen content and 3.6% hydroxyl groups. It is a chemical substance with a high absorption rate [14]. The formed polyacrylamide (PAAm) is a linear water-soluble polymer sensitive to temperature and pH. Polyacrylamide lacks biological activity and weak chemical qualities [15]. Nevertheless, it possesses advantages like high adhesiveness, appropriate hygroscopicity, and high hydrophilicity [16]. This polymer has recently been used in surface grafting polymerization and other current applications such as oil recovery, mining, and water treatment [17]. Further, PAAm is utilized as a flocculant and a material thickener. Producing tissue covering burns, prosthetic retinas, and soft tissues [18]. One of the biocompatible, hydrophilic polymers is polyvinyl pyrrolidone (PVP), which will be utilized for various biological applications and separation activities to augment the solubility of comprising polymeric materials mixed [19]. PVP has the real benefit of being thermally crosslinked, which increases the material's mechanical strength. Additionally, because PVP melts when exposed to water, it has promised to prevent phase separation in blends. The presence of long chains and carbonyl (C = O) groups in PVP make it an effective capping factor for nanoparticles. It is possible to alter the physical properties of polymers and include new features in a polymer blend by mixing inorganic NPs with polymers [20]. Water solubility, biodegradability, biocompatibility, non-toxicity, strong dielectric (> 1000 kV/mm), strong capacity to store charges, dopant-dependent electrical property, and non-carcinogenicity are just some of the exceptional properties of polyvinyl alcohol (PVA), a polymer with the ability to create hydrogels to use various methods [21, 22]. Commercially, it is produced by hydrolyzing polymers (vinyl acetate). Among other uses, PVA has been extensively employed as a thermoplastic polymer in living, non-toxic, and safe tissues. Many studies have investigated using PVA as fillers or crosslinking products [23]. PVA is a good anti-aggregation shield for nanoparticles [24]. Therefore, this investigation used PVA as a linker between the polymers and the NPs. H. They are frequently employed in producing paper, textiles, oxygen-retardant films, and coating photographic film [25].

Wang Y. et al. (2018) [2] reported preparing ternary blend solar cells. Poly(3-hexylthiophene) (P3HT), [6, 6]-phenyl-C61-butyric acid methyl ester (PCBM), diketopyrrolopyrrole (DPP), and carbazole (Cz) units used to prepare a ternary low-bandgap polymer (PCDPP4T). The results showed an increase in the photocurrent and power conversion efficiency. This improvement in photocurrent was ascribed partly to the near-infrared (near-IR) absorption region CDPP4T. Also, they reported a part of efficient energy transfer from P3HT to PCDPP4T. These ternary blend polymers significantly improve compared to P3HT/PCBM binary reference cells. M. Ragab and A. Rajeh, 2020 [26] reported a promising technique for producing polyacrylamide (PAAm) and chitosan (Cs) nanocomposite polymer systems. Hosting polymer for Ag/Se nanofiller in applications involving electrical energy storage. They reported a reduced optical energy gap, implying enhanced optical characteristics. The AC behavior was examined using the nanocomposites' frequency-dependent AC conductivity. The sample's ionic conductivity improved as the Ag/Se concentration rose, improving nanocomposite ionic and optical conductivity. Nanocomposites were appropriate for electrochemical applications, such as energy storage, elastic capacitors systems, and battery separators. Gaboury, L. (2019) [27] fabricated nanocomposite from chitosan and polyacrylamide containing silica nanoparticles (SiO_2) -based nanocomposite. The Cs/PAM blend's semi-crystalline nature is present. Due to the Cs/PAM blend matrix's masking impact brought on by the low amount of SiO_2, no peaks identifying SiO_2 have been present. The primary IR bands observed correspond to the functional groups for Cs/PAAm. After the SiO_2 nanoparticles were added, the positions of the IR bands remained unchanged. A 253 nm absorption band revealed the Cs/PAM matrix's semi-crystalline structure with a strong absorption edge in the UV–vis spectra. The optical characteristics of the spectrum were

recorded and described as a photon energy function. Alsaad AM et al. [28] used the dip-coating method, silica nanoparticle with weight percentages of SiO_2 NPs = 2%, 4%, 8%, and 16%)- based on PVA and PMMA. The optical transparency is significantly reduced when SiO_2 NPs are introduced into the PMMA-PVA matrix at certain concentrations. Tarek S. Soliman et al. (2020) [29] integrated different concentrations from 1 to 10% of the SiO_2 nanoparticles into polyvinyl alcohol (PVA) polymer for optoelectronic applications using a sonication technique and a solution casting approach. The XRD readings confirmed the semicrystalline character of the PVA. The SiO_2 nanoparticle homogeneity of the SEM was verified in the polymer matrix results. The films made of nanocomposite materials showed better thermal stability than polymer. The contribution of the increase of SiO_2 reduced the direct optical band gap and Urbach energy. At the same time, the extinction coefficient and refractive index were improved. Al-Asbahi, B. et al. (2021) [1] reported the impact of SiO_2/TiO_2 nanoparticles on the photoelectric properties for PFO/MEH-PPV/ F7GA ternary hybrid film using solution blending and spin-coated method. Incorporating nanomaterials exhibited charge transfer in the ternary system and improved charge carrier mobility. These improved the performance of the organic light-emitting and the current and decreased activation energy and resistance of the fordiode device. A. M. Mansour et al., 2022 [30] investigated the bandgap of SiO_2:ZnO: TiO_2 nanocrystallites prepared using the sol–gel route and co-firing at 600 °C temperature. This temperature calcined involves the $ZnTiO_3$, Zn_2SiO_4, and $ZnTiO_3$ leading rhombohedral phase, which displays several electronic transitions and indirect bandgap transition of 2.8 eV and 3.35 ± 0.01 eV, respectively, with the increase the ratios of silica. The AC conductivity is between 10^{-10} to 10^{-7} S/cm, and the dielectric constant is eight at a frequency higher than 10^4 of Zn_2SiO_4.

Many investigations [1-3, 27-31] showed that the raw materials of SiO_2 and the oxide additions have different particle sizes and densities are the key factors for changing the properties of the polymers [31]. Advanced peaceful materials are widely listed in rubber, plastic, and polymers, but they suffer from several problems and need improvements using nanomaterial [7]. There are several applications, including biological, antibacterial activity, and electrical applications, such as sensors for light, heat, etc. [9, 11, 32].

Even though several studies [1, 27-30, 33] investigating the effect of SiO_2 nanoparticles, PAAm, PVA, and PVP polymers were not mixed as ternary hybrid blended polymers or integrated with different loading ratios of SiO_2 nanoparticles to the best of our knowledge. There is a very limited investigation focused on ternary hybrid blended polymers. In addition, these factors are still not fully understood and need many investigations to cover these influences. Therefore, these investigations focused on newly fabricated different ratios of three ternary hybrid blended polymers with different loading ratios of SiO_2 nanoparticles for optoelectronic and antibacterial activity applications. The nanocomposites were investigated with various characterizations to examine their structure, morphology, optical and electrical properties, and antibacterial activity.

2 The Experimental Part

2.1 Materials

PAAm with an Mw. of (71.07) g/mol, formula: $(C_3H_5NO)_n$ white color, and crystal-granular appearance supplied from Wuxi Lansen Chemicals Co., Ltd, China. PVA with an Mw of (160,000) g/mol and molecular formula: $(C_2H_4O)_n$ provided from Dindori, Nashik, India. The Mw of PVP is (40,000) g/mol, linear formula $(C_6H_9NO)_n$, white color to light yellow, and hygroscopic, delivered by Alpha chemical company, India. SiO_2 nanopowders with grain size (of 20–30) nm, white color, purity of (99.8%) melting point of (1610–1728 °C), and boiling point range (of 2230 °C), supplied from Hongwu Inter National group ltd, China.

2.2 Methods

2.2.1 Preparation of Blended Polymers and Nanocomposites

Independently, polymers were dissolved, and SiO_2 nanomaterials were dispersed in distilled water (DW). The polymer mixture was fabricated using different proportions of polymers (45:10:45) for PAAm:PVA: PVP. Firstly, 10 wt.% of PVA/DW was added after dissolving in distilled water to 45 wt.% of PAAm/DW and combining the mixture for two hours. Secondly, PVA was added in this stage to increase the interaction between the polymers. It is considered a factor that strengthens the link between the polymers. Thirdly, PVP/DW with 45 wt.% concentration was added to the PAAm-PVA matrix and blended for two hours to fabricate PAAm-PVA-PAA using the magnetic stirrer to achieve BP1. Fourthly, the nanocomposites were prepared following the same procedure by adding different ratios of SiO_2 (0.01, 0.03, and 0.05) wt. %. Finally, the samples matrix was placed in a petri dish (5 cm) and dried in the vacuum oven at 40 °C for 73 h until fully dried. Samples were saved in the desecrator till characterizations were done. The samples were coded simply according to the nanomaterial's ratios, as shown in Table 1, and the procedure is presented in Fig. 1.

Table 1 Displays mixing weight percentages of samples

Sample ID	Concentration wt. %			
	PAAm	PVA	PVP	SiO_2
BP1	45	10	45	0.00
NC2	45	9.99	45	0.01
NC3	20	9.97	70	0.03
NC4	70	9.95	20	0.05

2.3 Characterizations

Table 2 Summaries the characterizations employed in this investigation.

The term absorbance (A) refers to the percentage between the absorbed light intensity (I_A) to its incoming light intensity (I_o) in the materials. That is given in the following equation [34].

$$A = \frac{I_A}{I_o} \tag{1}$$

T is transmittance and is calculated by the relation [34].

$$T = \log A \tag{2}$$

To calculate the absorption coefficient (α), Eq. 3 was applied [35].

$$\alpha = 2.303^{A}/_{t} \tag{3}$$

where (t) means the thickness of the sample. There is a specified energy gap calculated by [36].

$$\alpha h\upsilon = B(h_{\upsilon - E_g})r \tag{4}$$

where (B), (hυ), and (E_g) mean constant, photon energy, and the energy gap, respectively, whereas r = 2 and 3 to permitted

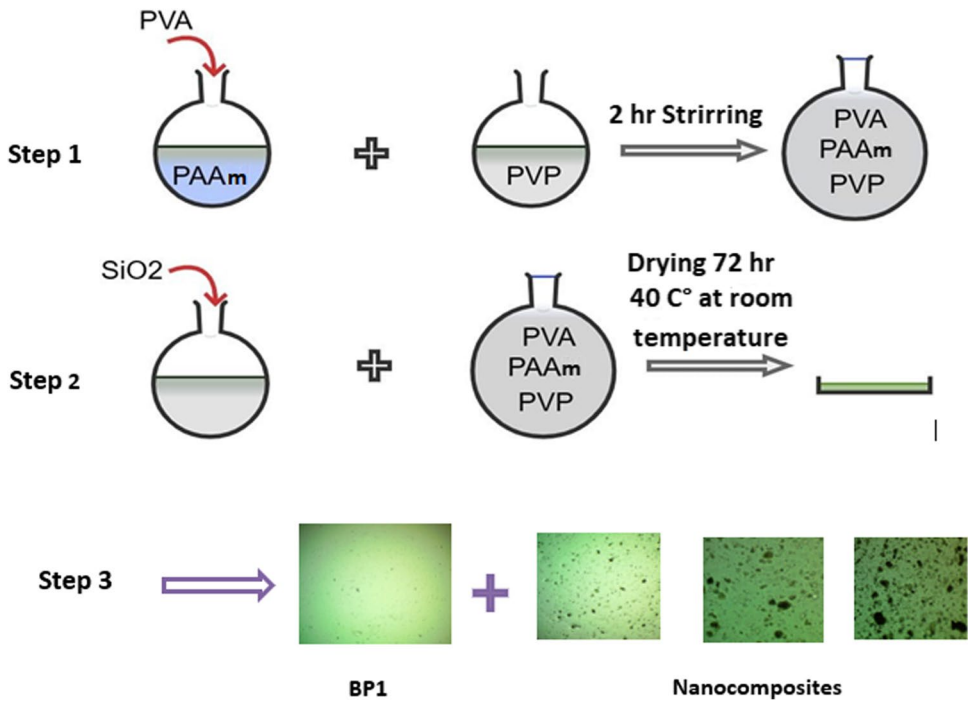

Fig. 1 Scheme of the experimental work procedures of fabricated sample films

Table 2 Outlined the characters' traits that were employed

Device	Model	Details	Manufacturing and State
FTIR	vertex 70	Range, 4000 -500 cm^{-1}	Bruker Company, Germany
X-rays	Powder XRD, DX2700PH, multi-function x-ray	Current 0–80 MA, Voltage 0–60 kV, Cu target 1.50 nm	Haoyuan instrument co. ltd
OMI	Nikon 73,346	40X Magnification	Olympus Company, Japan
FE-SEM	TESCAN	Veg	Tescan company, Czech Republic
UV–Visible	Vertex 701	Double beam	Phillips Company, Japan
AC Electrical	Hi TESTER, (3532–50)	LCR meter	Hioki, Japan

and prohibited indirect transitions. As stated, the refraction index (n) is specified by Eq. (5) [37].

$$n = \frac{1 + \sqrt{R}}{1 - \sqrt{R}} \tag{5}$$

where (R) and (k) are the reflectance and extinction factor that is given [38]:

$$k = \frac{\alpha\lambda}{4\pi} \tag{6}$$

(λ) means the wavelength, whereas the real dielectric (ε_1) and imaginary (ε_2) constants are given by Eqs. (7 and 8) [39].

$$\varepsilon_1 = n_{2\_}k_2 \tag{7}$$

$$\varepsilon_2 = 2nk \tag{8}$$

The optical conductivity (σ_{op}) is defined by relation (9) [40].

$$\sigma_{op} = \alpha nc/4\pi \tag{9}$$

where (c) means the light velocity. The dielectric constant (έ) is given by [41].

$$\acute{\varepsilon} = \frac{C_P}{C_o} \tag{10}$$

(c_p) means the parallel capacitance, and (c_o) means the vacuum capacitor.

Dielectric loss (ε˝) is calculated by Eq. (11) [42]

$$\varepsilon^{\varepsilon} = \acute{\varepsilon}\, D \tag{11}$$

D means the dispersion factor.

3 Results and Analysis

FT-IR spectroscopy is one of the main tools that provide information to help recognize the interconnections between the matrix functional groups and their interactions to identify the mixture and the nanoparticles at the intermolecular level. The FTIR spectrum in pure PAAm in Fig. 2A, the broad band observed at 3329 and 3182 cm^{-1}, is linked to the asymmetric variation of NH_2 and symmetric vibration of NH_2. The two intense peaks at 2908 and 2321 cm^{-1} correspond to the CH_2 asymmetric stretching and strong O=C=O stretching vibration. The two peaks are 1651 and 1604 cm^{-1} due to the C=O vibrational stretching and N–H bending [43]. In the FTIR spectrum for pure PVA in Fig. 2A, the broad band observed at 3278 cm^{-1} is linked to the stretching O–H from intramolecular hydrogen bonds [44]. The two intense peaks at 2908 and 2320 cm^{-1} correspond to the CH_2 asymmetric stretching and O=C=O stretching vibration. The peak at 1711 cm^{-1} is due to the stretching C–O from the carbonyl group, and the peak at 1361 cm^{-1} corresponds to the C–H deformation vibration. The peak at 1244 cm^{-1} is attributed to the deformation stretching vibration of the C-N link. Moreover, the peaks observed at 1089 and 850 cm^{-1} could be attributed to the twisting vibration of the strong

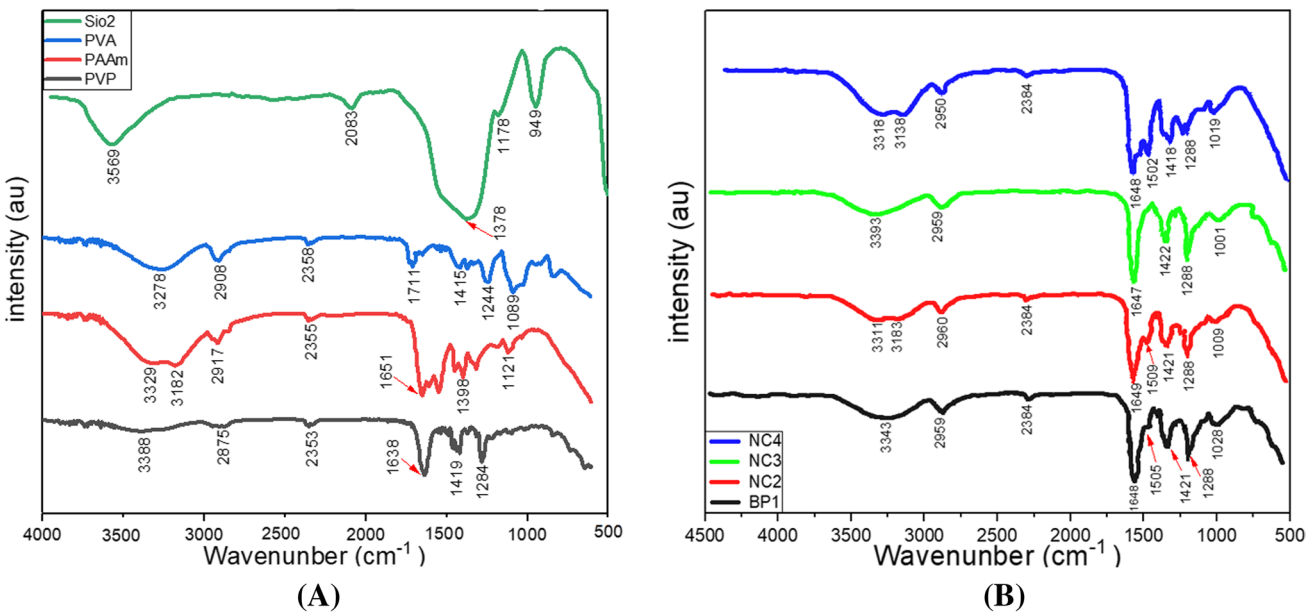

Fig. 2 FTIR spectrum of (**A**) polymer and SiO_2 and (**B**) nanocomposites

C-O stretching vibration band and medium C = C bending [45, 46]. Three peaks at 1398, 1290, and 1120 cm^{-1} correspond to the CH_2/CH group, CH_2/CH moiety, and CH_2/CH group, respectively [47]. The FTIR spectrum of PVP in Fig. 2A had a peak at 3388 cm^{-1}, which indicates O–H stretching. The peaks at 2903, 2321, and 1652 cm^{-1} proved the existence of asymmetric stretching of CH_2, O = C = O stretching vibration, and stretching of C-O, respectively. The C-H bending and CH_2 wagging was observed at 1419 cm^{-1} and 1284 cm^{-1}, respectively. The peak at 1089 cm^{-1} was identified as the N–C = O bending [48]. In the FTIR spectrum in pure SiO_2 in Fig. 2A, the broad band observed at 3569 cm^{-1} is linked to the stretching O–H from intramolecular hydrogen bonds. The two intense peaks at 2083 cm^{-1} correspond to the CH_2 asymmetric stretching and O = C = O stretching vibration. The peak at 1711 cm^{-1} is due to the stretching C–O from the acetate group, and the peak at 1378 corresponds to the C–H deformation vibration. The peak at 1178 cm^{-1} is attributed to the deformation stretching vibration of the C-N link. Moreover, the peaks observed at 949 could be attributed to the twisting vibration of the strong C-O stretching vibration band and medium C = C bending.

Figure 2B shows the FTIR spectrum of the ternary blend polymers BP1 and NC films with (0.01.0.03.0.05) wt. % of SiO_2 in range (500–4000) cm^{-1} wavenumber. Several peaks were observed in the BP1 spectrum that observed peaks at 3343, 2959, 2384, 1648, 1505, 1421, 1288, and 1028 cm^{-1} and was connected with the expansion hydroxyl (O–H) group and methylene oscillations (C-H_2), strong O = C = O stretching vibration, (C = C) stretching, (N–O) stretching, (O–H) bending, (C-O) stretching, and (C-O) stretching. The results of the PAAm-PVA-PVP/SiO_2 vibration pattern (NC2) revealed the same peaks, whereas some peaks were shifted to 3311 and 3183, 2960, 2384, 1649, 1509, 1421,1288, and 1009 cm^{-1}, in addition to present two peaks in the O–H area at 3311 and 3183 cm^{-1} than one abroad peak for BP1. Increasing the SiO_2 to 0.03 wt. % and change the ratios of polymers revealed shifting of the most peaks position to 3393, 2959, 1647, 1288, and 1011 cm^{-1}. Additionally, it noted one peak in the O–H area. The peaks at 2384 and 1509 cm^{-1} were dispersed, which could relate to increasing the PVP ratio of 70 wt. % as a higher ratio in this sample NC2. Increasing concentration of SiO_2 NPs to 5 wt. % and increasing the ratio of PAAm to 70 wt. % in the NC4 showed the same peaks of NC2. Most of the peaks were shifted to 2950, 1649, 1502, 1418, and 1019 cm^{-1}, respectively, compared with PB1. Also, it is noted increasing the intensity of some peaks 2384 and 1502 cm^{-1}. The FTIR spectrum of these polymer nanocomposite films demonstrated the interfacial interactions between the miscible chain architectures and the SiO_2 nanoparticles and PAAm-PVA–PVP blend. The presented functional groups approved the fabrication of BP1 ternary blend polymers and NCs, whereas the loaded of SiO_2 exhibited changes in the position peaks and intensity of such as O–H, C-O, and C-H as a result of the network formed between SiO_2 and oxygenated groups of polymers. These results strongly agreed with other reports [7, 11].

The crystallographic structure of polymers and SiO_2 was determined using XRD patterns, as shown in Fig. 3A. PAAm spectra display an amorphous structure with a broad peak between 10 to 50°, where the higher intensity of the top peaks was at 2θ = 22° with other small features exhibited

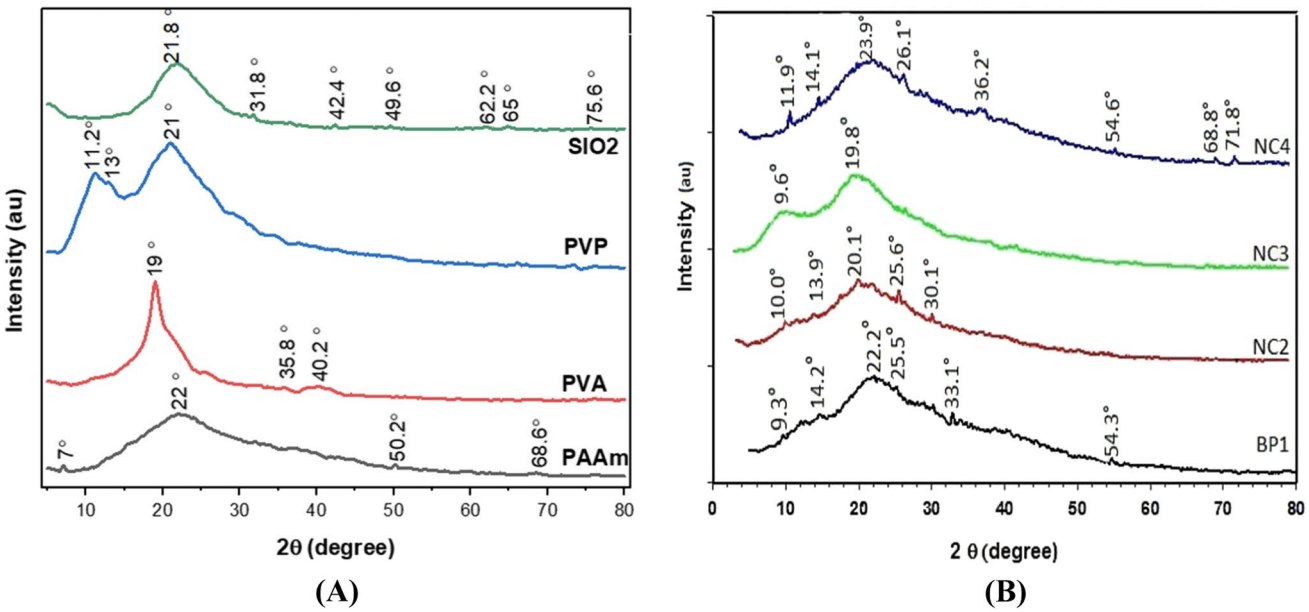

Fig. 3 XRD patterns of (**A**) polymer and SiO_2 and (**B**) nanocomposites

at 7°, 50.2°, 68.6° in agreement with the literature [46, 49]. PVA spectra display an amorphous structure with a broad peak where the higher intensity of the top peaks was at 2θ = 19° and other small features exhibited at 35.8°, 40.2° [9, 50]. PVP spectra display an amorphous structure with a broad peak where the higher intensity of the top peaks was at 2θ = 21°. Other small features were exhibited at 11.2° and 13° [51]. SiO_2 spectra display an amorphous structure with a broad peak where the higher intensity of the top peaks was at 2θ = 21.8°. Other small features exhibited at 31.8°, 42.4°,49.6°, 62.2°, 65° and 75.6° in agreement with other report [11].

The crystallographic structure of BP1 polymer blend and its nanocomposite films with different ratios of (1, 3, and 5) wt.% SiO_2 NPs were determined using XRD patterns, as shown in Fig. 3B. BP1 spectra display an amorphous structure with a broad peak between 10 to 50°, where the higher intensity of the top peaks was at 2θ = 22.2°. Other small features exhibited at 9.3, 14.2, 25.5, 33.1, and 54.3°.This behavior is similar to the PAAm-PVP behavior reported in the literature [33, 52]. PVA crystallite pattern at 19.9° disappeared, which could be overlapped in the abroad peaks, or the lower percentage could assist in this disappearing in agreement with the other reports [53, 54]. NC2 showed the same behavior as BP1, but the contribution of SiO_2 exhibited shifting in the top abroad peaks from 2θ = 22.2° to 20.1°, and 10.0, 13.9, 25.6 and 30.1°, respectively. Whereas NC3 revealed a different behavior than BP1 and NC2, NC3 exhibited two main peaks at 9.6° and 19.8°. This behavior matched the behavior of pure PVP because it consists of 70 wt. % of PVP in strong agreement with the literature [55]. It showed a reduction or diapered in the SiO_2 peaks presented in the NC2. NC4 showed the same behavior as BP1 and NC2. The contribution of the increase in the SiO_2 nanoparticle concentration to 0.05 wt. % showed a shift of the main top peak back from 2θ = 22.2° to 23.9°, in addition, another shifting of peaks from 9.3 to 11.9°, 25.5 to 26.1°, and 54.3 to 54.6°. Furthermore, it also revealed new small peaks at 2θ = 11.9, 36.2, 68.8, and 71.8º compared with BP1. NC4 showed an increase in the number of peaks from 5 to 8 compared with NC2 and from 2 to 8 compared to NC3. The ratios of both polymers and nanoparticles showed important factors that affected the behavior of nanocomposites as that presented the general behavior turned with the specific behavior of the higher ratio of main consist of the polymer as presented in the NC3 and NC4. Notably, incorporating SiO_2 nanoparticles considerably changes the crystallinity degree of PAAm-PVA-PVP blended polymers. In addition, presents the small features of crystalline peaks after increasing the concentrations of nanoparticles from 0.01 to 0.05 wt. %. This behavior is strongly agreed with other researchers who reported the impact of SiO_2 on the PVP/PVA/SiO_2 membrane [33].

Several factors could be estimated from the XRD peak position to comprehend the XRD outcomes of the samples better. Bragg Eq. (12) was implied to calculate the interplanar d-spacing [56].

$$n\lambda = 2d\sin(\theta) \tag{12}$$

(n), (λ), (d), and (Θ) refer to the integer, the wavelength, the incident angle, and the X-ray and the scattered beams, respectively. The crystallite size (D) in nm is measured using the Scherrer formula (13) [57].

$$D = k\lambda/\beta\cos(\theta) \tag{13}$$

The crystal means, and the complete breadth at half the highest point (FWHM) (k = 0.9) are factors (2), according to Table. The lattice strain (ε) can be calculated using Eq. (14) [57].

$$\varepsilon = \beta/4\tan(\theta) \tag{14}$$

As the amount of SiO_2 nanoparticles in the matrix's structure increased, the samples' crystallite sizes (D) increased. D was raised from 0.834 to 1.253 nm in that location. Furthermore, as shown in Table 3, the contribution of the nanoparticles (2) affected the (D).

The optical images of PAAm-PVA-PVP blended polymers and PAAm-PVA-PVP/SiO_2 at magnification 40X are shown in Fig. 4**.** These images illustrated good homogeneity and the distribution of SiO_2 with some aggregations into the polymer blend, which means a good procedure for preparing the blended polymers and PAAm-PVA-PVP/SiO_2 nanocomposites. Nanocomposites showed a noticeable alteration with an increase in the SiO_2 ratios. The influence of SiO_2 revealed several changes in all of these films, with some aggregates in the films without effects on the films' transparency, as shown in the inset images in Fig. 4, in agreement with others finding [58, 59].

FESEM examined the surface morphology and dispersion of the nanoparticles in the polymer matrix, as exposed in Fig. 5. Samples presented the nano communications polymers viewed on the sample's surface (left side) with micron-size (right side) nanosized images, as revealed in Fig. 6. Pure polymer membranes (BP1) (left side) showed homogeneous, grainy, coarse surface shapes. The right side shows that the surface suffers from some cracks and that the polymer crystals. On the left side, SiO_2 nanoparticles with 0.01 concentration in the NC2 revealed affected the polymer matrix and showed good dispersion of nanoparticles with granular structure but without assemblies. (Right side) revealed that the surface was rough and homogeneous, but the crack still appeared. Increasing the load ratio of SiO_2 nanoparticles to 0.03 and 70 wt. % of PVP represented the grainy surface of the NC3 (left side). Meanwhile, on the (right side), crack numbers and size were generally reduced.

Table 3 Summarizes the size of the crystallites, typically FWHM, diffraction angle, and nanocomposite and mixed polymer lattice strain

Samples	2θ (˚)	d (nm)	β (°)	D (nm)	Average crystallite size D_{avarge} (nm)	Lattice Strain * 10^{-3}	Average Lattice Strain * 10^{-3}
BP1	9.3	0.894	0.951	7.840	7.83	0.051	0.027
	14.2	0.586	1.439	5.158		0.050	
	22.2	0.376	1.087	6.753		0.024	
	25.5	0.328	0.765	9.538		0.014	
	33.1	0.254	1.306	5.491		0.019	
	54.3	0.158	0.786	8.470		0.006	
NC2	10	0.832	0.822	9.066	10.5	0.040	0.024
	13.9	0.599	0.846	8.777		0.030	
	20.1	0.415	0.689	10.691		0.016	
	25.6	0.327	1.502	4.856		0.028	
	30.1	0.279	0.649	11.131		0.010	
NC3	9.6	0.866	1.125	6.626	7.5	0.058	0.040
	19.8	0.421	0.956	7.708		0.023	
NC4	11.9	0.699	0.53	14.038	7.62	0.022	0.018
	14.1	0.590	0.942	7.881		0.033	
	23.9	0.370	1.087	7.592		0.021	
	26.1	0.321	1.011	7.208		0.019	
	36.2	0.233	1.581	4.497		0.021	
	54.6	0.158	1.494	4.450		0.012	
	68.8	0.128	1.339	4.610		0.008	
	71.8	0.123	1.792	3.382		0.010	

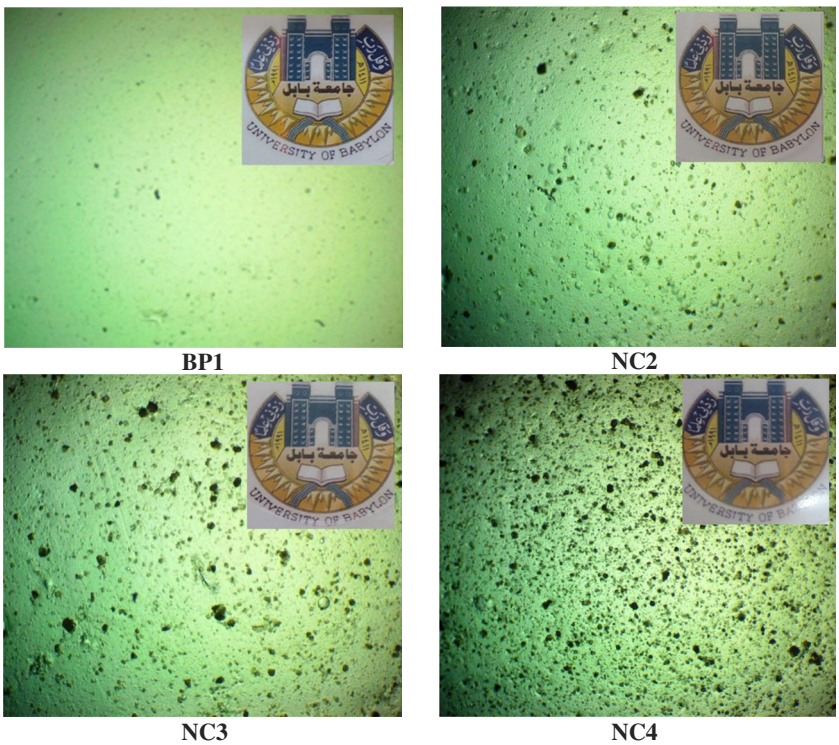

Fig. 4 Photomicrographs of OPM (40X) and inset images for samples

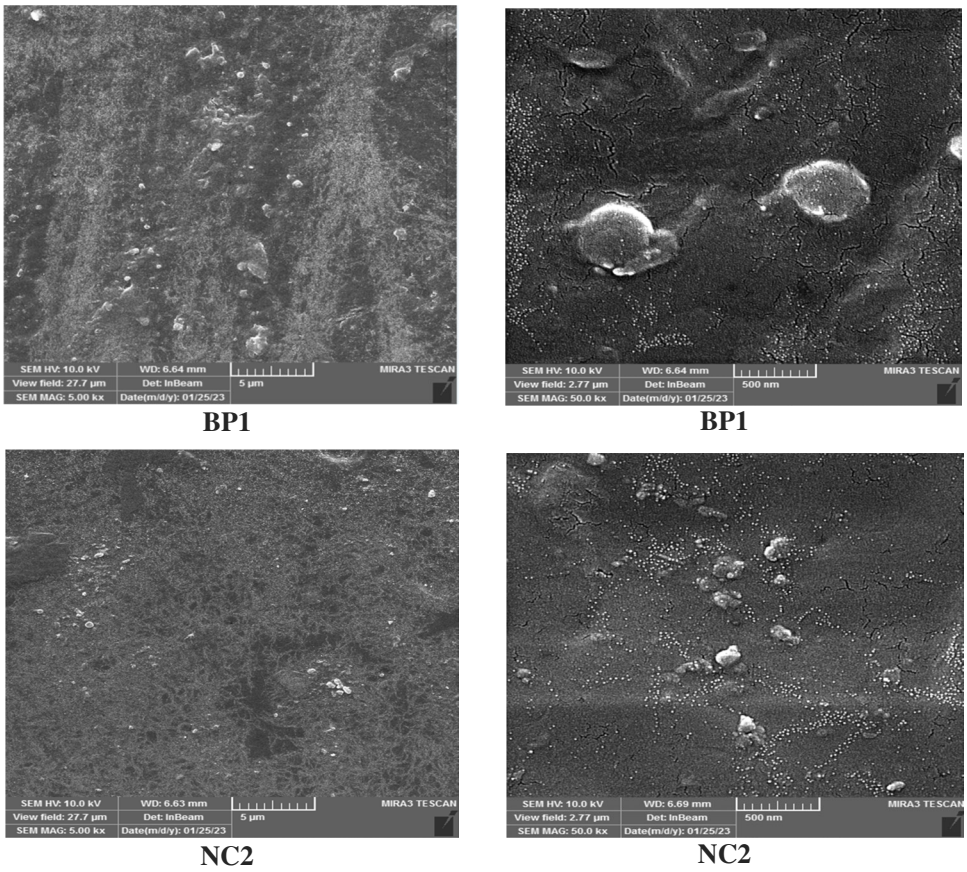

Fig. 5 FESEM (left side) and FESM (right side) images of samples

The incorporation of increasing nanoparticles to 0.05 wt. % and PAAm to 70 wt. % in the NC4, FSEM images on (the left side) showed a rough, coarse surface. Interestingly, the cracks in the NC4 surface were significantly reduced too difficult to recognize and became very smooth compared with other samples. Moreover, the surface of the NC4 showed the type of specific shape order or type of semi-crystalline shape of polymer particles existing on the surface. This supported the existence of crystalline peaks in the NC4 compared with other samples. Another observed the SiO_2 appeared on the surface of the samples that started reducing in NC3 and diapered in NC4. This could referee good adhesions and stronger interfacial interaction of the NC4 in agreement with FTIR results that showed a change in the functional peaks and XRD results.

Figure 6 shows the optical absorbance in the range of (200–1100) nm wavelength range samples. All samples had higher absorbance values in the UV band. The donor electrons were conduction band excitations at high energies by taking in a photon with known energy. The donor electrons were excited energy level increased from lower to higher. Additionally, the outcomes demonstrated a strong photon absorbance by the samples in the UV area. This resulted in these photons having sufficient to exert energy on atoms, especially at 200 nm. At high energies (200 nm), the sharp absorption peak could relate to the transition of plasmonic π-π^* stacking (C = C) or the covalent bonding that indicated the interaction between the component's matrixes. This result matches the functional group with strong (C = C) vibration at 1648 cm^{-1}.

Where increasing the contribution of the loading ratio of nanoparticles from 1 wt. % to 5wt. % SiO_2 NPs and PAAm from 20 wt. % to 70 wt. % revealed an enhancement in the absorbance from 0.73 to 0.91 with 25%. Whereas, at higher wave numbers between (340 to 1100 nm), the absorbance values were also improved from 0.013 to 0.113 at 1100 nm. Also, it is not that the increasing wide of the absorption peak increased that begin absorption from 260 nm then increased up to 320 nm. This may be connected with the incident photons' inability to interact with atoms because they lack sufficient energy and the transmitted photon at high wavelengths. These findings agreed with the literature [28, 60, 61]. SiO2 nanoparticles exhibit an abrupt reeducation in the (0–400 nm) low UV region suggesting strong electron transition within the bandgap [28]. The red shift toward high wavelengths suggests an electronic transition from $n \rightarrow \pi^*$ and confirms the complexation process between ternary blend polymers and SiO_2 nanoparticles [46]. Ternary blend polymer concentrating does not show a strong effect on the results. At the same

Fig. 5 (continued)

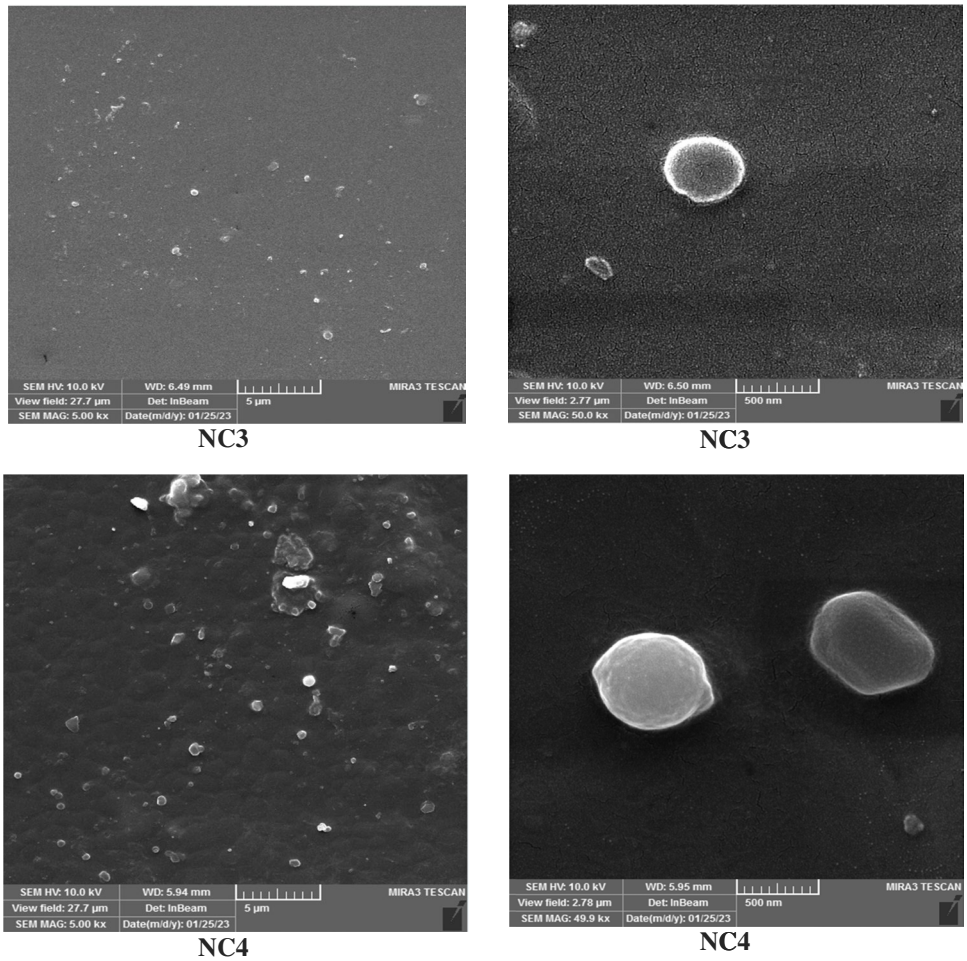

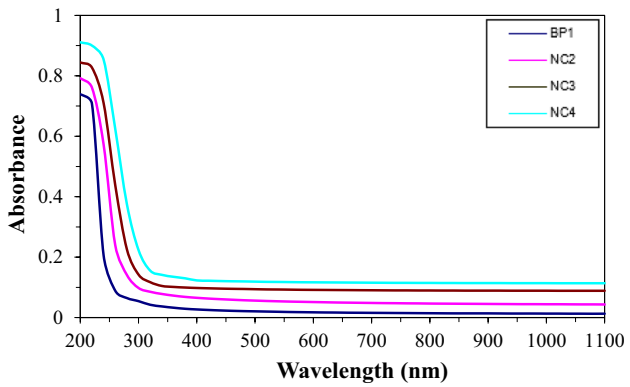

Fig. 6 Absorbance spectra with a wavelength of the sample

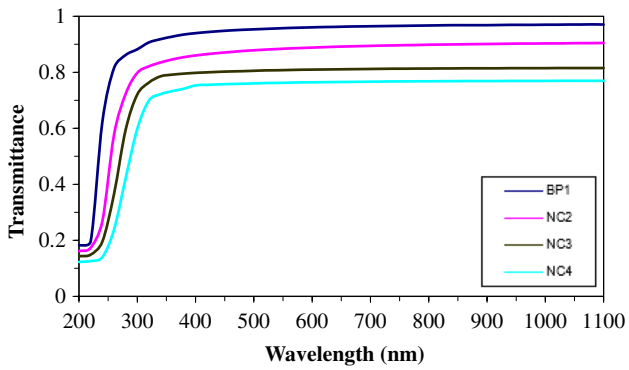

Fig. 7 The transmittance spectrum with a wavelength of samples

time, the results demonstrated reduced results with boosting the amount of SiO_2 in the matrix. Increasing the nanomaterials could increase light absorbance while decreasing transmittance for the same reason [62]. Additionally, the shift indicates an increase in the conjugation lengths of the polymers in agreement with the other finding [1]. Despite increasing the absorption of light amount, this did not impact the transparency of the samples, as shown in the inset optical images in Fig. 4.

The transmittance was considered from relation (2). Figure 7 shows T spectra with the samples' wavelength. The transmittance behavior for all samples was rapidly raised with increasing the wavelength at about 240 nm, and then it was steady after 280 nm. Polymer concentrating does

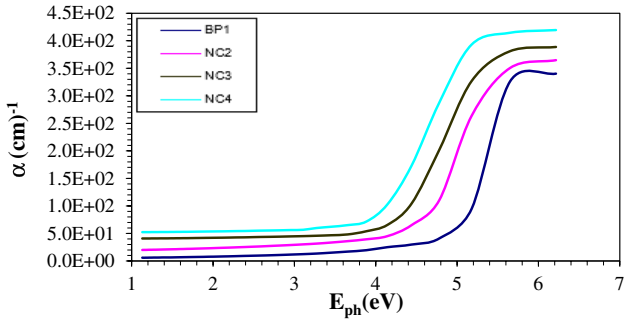

Fig. 8 Absorption coefficient with the photon energy of samples

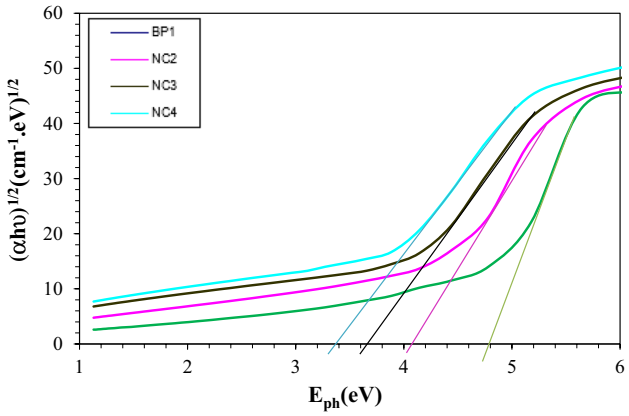

Fig. 9 Tauc optical energy gap of the allowed indirect transition with the photon energy for samples

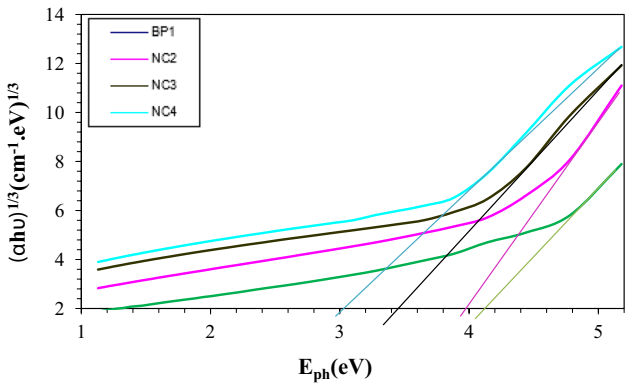

Fig. 10 Tauc optical energy gap of the forbidden indirect transition with the photon energy of samples

not show a strong effect on the results. At the same time, the results demonstrated reduced results with boosting the amount of SiO_2 in the matrix. Increasing the nanomaterials could increase light absorbance while decreasing transmittance for the same reason [53].

Figure 8 displays the impact of SiO_2 nanoparticles on the absorption coefficient (α) of sample films with photon energy. The absorption coefficient (α) was considered from Eq. (3). The behavior of the absorption coefficient showed a constant increase in values with increasing photon energy to about 4 eV of most samples. This may be connected to the electron's lower transition, where to transfer from the electron of the conduction band to the valence band, more input photon energy was required. In contrast, the absorption coefficient rapidly increases after 4.6, 4.2, 4, and 3.8 eV of BP1, NC2, NC3, and NC4 to reach 340, 362, 388, and 420 cm^{-1} at 6.2 eV, respectively. Increasing the SiO_2 nanoparticles in the polymer matrix is linked with increases in the absorption amount; at lower energy (1 to 4 eV), the absorption coefficient enhanced from 23.3 to 53.6 cm^{-1}, and at higher energy (4 to 6.4 eV) 340.2 to 419.4 cm^{-1}. The increasing outcomes result from the strong electron transitions in the conductive band and scattering induced by the SiO_2 in the ternary matrix, as rise with an increase in the amount of SiO_2, which is promising for optoelectronics and solar cell applications in agreement with the literature [1, 11].

Figures 9 and 10 exhibit the indirect band gap of permitted $(h)^{1/2}$ and Prohibited $(h)^{1/3}$ of PAAm-PVA-PVP and PAAm-PVA-PVP/SiO2 with the power of photons. These values were estimated using the formula (4) with $(hv)^{1/2}=0$. Using the intercept of the extrapolated linear portion. A straight line was drawn from the curve's upper portion in Figs. 9 and 10 to consider the energy gap. This figure shows that the energy gap significantly reduced with increasing concentration of SiO_2, as shown in Table 4. It is reduced from 4.8 eV for PAAm-PVA-PVP blended polymers to 3.4 eV for PAAm-PVA-PVP/SiO_2 nanocomposites for the allow band gap. The forbidden band gap exhibited a reduction in the value from 4.2 eV for PAAm-PVA-PVA-PVP to 3.1 eV polymer mix for PAAm-PVA-PVP/SiO_2, as a result

Table 4 The optical energy gap of samples

Samples	E_g of Allowed Indirect (eV)	E_g of Forbidden Indirect (eV)
BP1	4.8	4.2
NC2	4.1	3.9
NC3	3.6	3.5
NC4	3.4	3.1

of polymer ratio manipulation and increased load ratio from 0.00 to 0.05 wt.%. The contribution of SiO_2 NPs was displayed as an important factor in the adjustable range gap.

Additionally, raising the load ratio of SiO_2. This revealed a significantly reduced in the energy gap values in non-communications. The energy gap is reduced by increasing the concentration of nanomaterials. This is because of the rise in the positioning levels between the parity and delivery packages. In this scenario, the electron moves from the parity package to the positioning levels and then to the two stages.

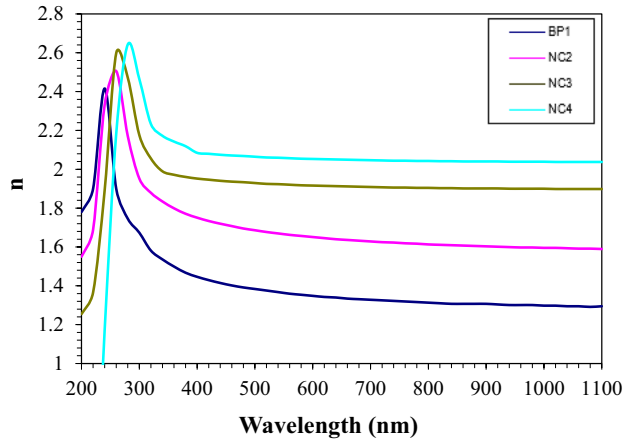

Fig. 11 Refractive index with wavelength samples

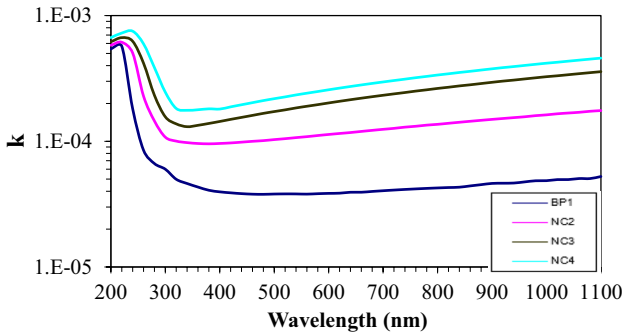

Fig. 12 The Extinction coefficient with the wavelength of samples

The positioning levels of the connectivity package agree with other finding [60, 63].

Figure 11 demonstrates the refraction index curves of samples with the desired wavelength. The refraction index (n) was calculated from relation (5). The reflect index presented a high value at a lower wavelength, which was reduced gradually with increasing the wavelength. The loading of SiO_2 to the NPs nanocomposites increased the samples' refractive indices. The density of nanocomposites may be increasing, which could explain this phenomenon in agreement with other finding [64, 65]

Figure 12 illustrates the samples' wavelength-based extinction coefficient (K). The extinction coefficient (K) was considered from the relation (6). In the UV area, nanocomposites revealed a greater extinction coefficient value, connected to the high absorption for every nanocomposite. The same effect also exhibits in the visible and near-infrared spectrum. These findings showed that adding SiO_2 NPs to the polymer mixture considerably improved the behavior of the nanocomposites.

The real and hypothetical dielectric constant was measured from relation (7). The relationship between

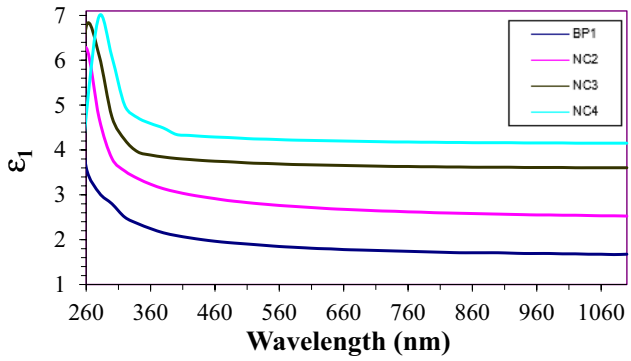

Fig. 13 The real dielectric constant with wavelength for samples

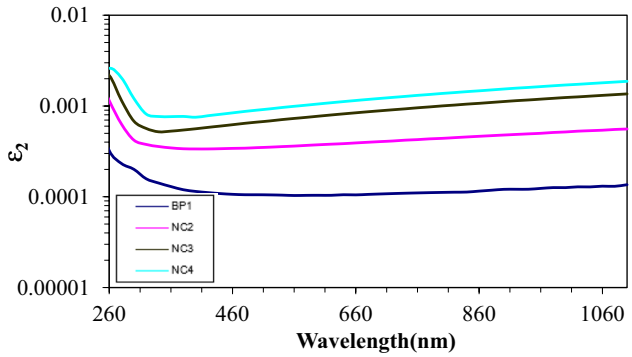

Fig. 14 The imaginary dependence dielectric is constant with the wavelength for samples

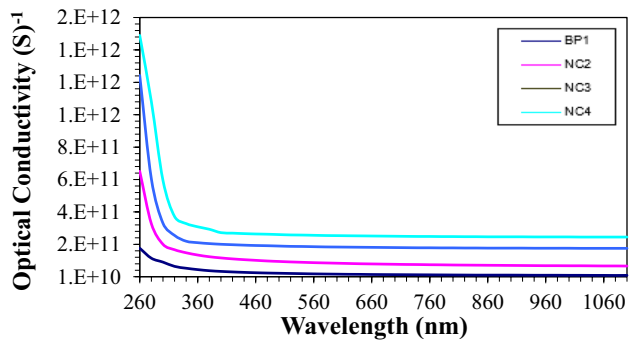

Fig. 15 Variation of σ_{op} with the wavelength for samples

the wavelength and the actual and imaginary dielectric constant of the PAAm-PVA-PVP/ SiO_2 nanocomposite is illustrated in Figs. 13 and 14. These graphs demonstrate how raising the SiO_2 to NP concentration ratio enhanced both portions' real and fictitious dielectric constants. The nanocomposites' increased electrical polarization is to blame for this. Optical conductivity was calculated using Eq. (8). The σ_{op} for the samples with a wavelength is demonstrated in Fig. 15. From this fig, the σ_{op} enhanced with

increasing the content of SiO_2 NPs in the matrix, which is connected to the formation within the localized energy gap, rising nanoparticle content induced rise in the band structure's density of localized phases. Therefore, a higher absorption coefficient indicates a higher in σ_{op} of the nanocomposites. This outcome is consistent with a previous study [66] and promising for solar cell applications [3].

The dependence dielectric constant was calculated from relation (8) for (PAAm-PVA-PVP/SiO_2) nanocomposites that are depicted in Fig. 16 A. The graph indicates redaction in the dielectric constant values as the applied frequency rises. This could relate to the polarization of space charges relative to the total polarization decrease. Space charge polarization contributes more to the electric field at low frequencies and less at higher frequencies, which would cause the dielectric constant values for every instance for nanocomposites to drop as the electric field's frequency increases [63]. Where Fig. 16 B displays constant dielectric changes with increasing the concentration of SiO_2 NPs. The weight percentages of SiO_2 NPs grow together with the dielectric constant, which causes the increase. Creating a continuous network of SiO_2 NPs ions inside the composite and the charge carriers. This finding agrees with other publications' previous findings [7, 67].

The dielectric loss was calculated from Eq. (9), revealed in Fig. 17A. Figure 17A demonstrates the relationship between dielectric loss for samples and frequency. The behavior values of dielectric loss showed a redaction with increasing frequency. This could be explained according to the space charge polarization contribution decreased as frequency rise, where the highest value of the dielectric loss is presented at a low frequency of f = 100 Hz and then reduced with increasing frequency. This figure shows an applied field's highest dielectric loss, or greatest absorption, at a particular frequency. Because the phases of nanocomposites have different dielectric constants and conductivities, the absorption occurs due to the Maxwell–Wagner phenomenon carried on by A.C. current [65]. Figure 17B shows the correlation between silica content and dielectric loss. It is obvious from the figure that the notable increase in values of the charge carriers was brought by an increase in SiO_2 NPs concentration. This behavior follows previous studies [68].

AC electrical conductivity was intended from relation (10) and revealed with frequency in Fig. 18A. As shown in the figure, the space charge polarization at low

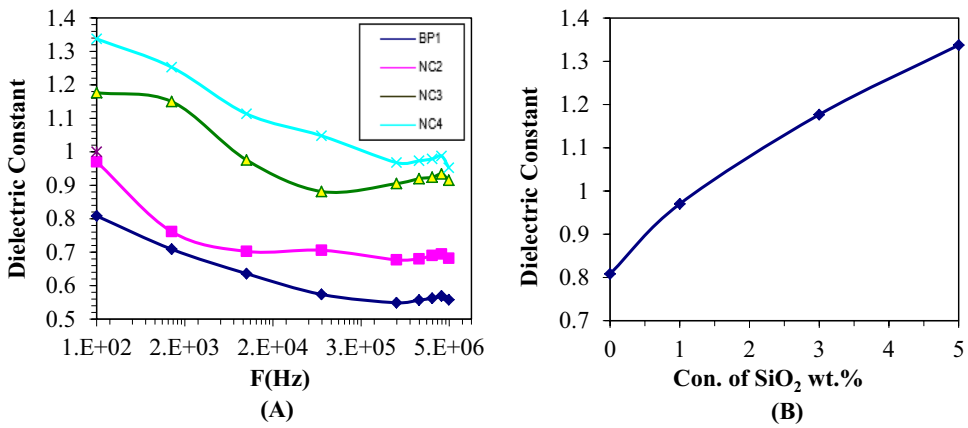

Fig. 16 Dielectric constant variation with (**A**) frequency and (**B**) the concentration of SiO_2 NPs for samples

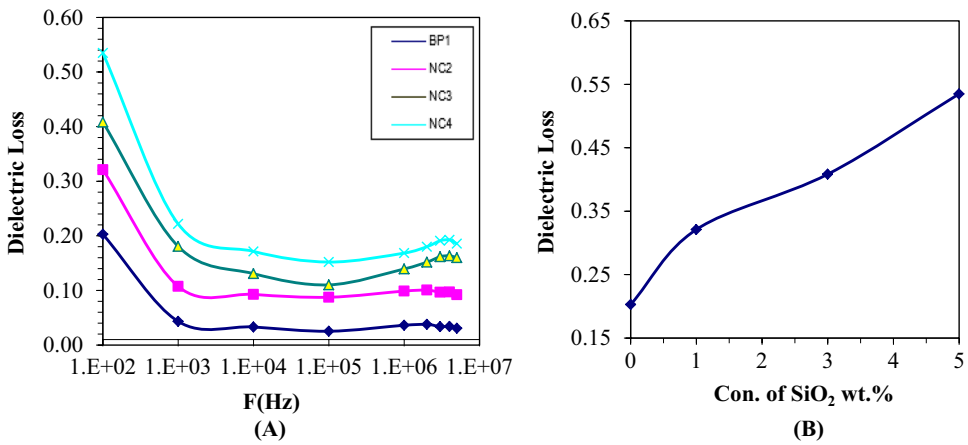

Fig. 17 Relationship between dielectric loss with (**A**) frequency and (**B**) concentration of SiO_2 NPs for samples

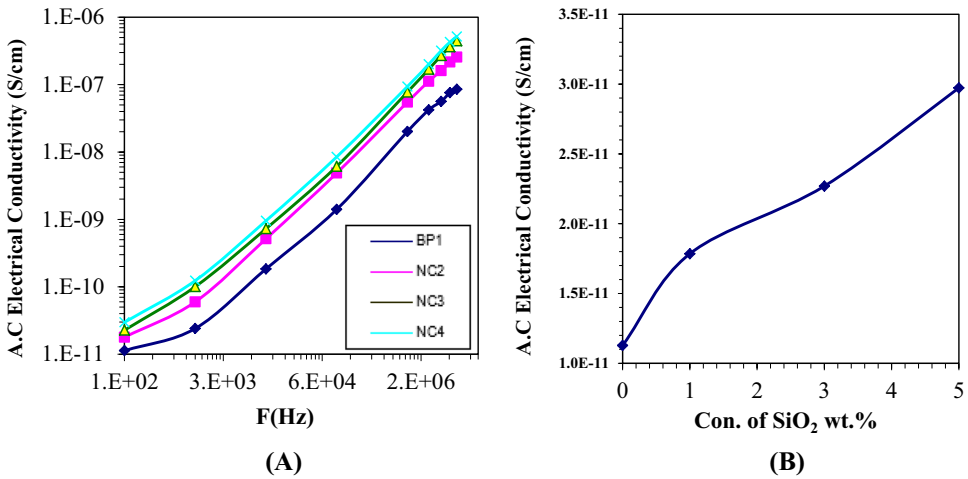

Fig. 18 The dependence on A.C. electrical conductivity (**A**) with frequency and (**B**) the concentration of SiO_2 NPs of samples

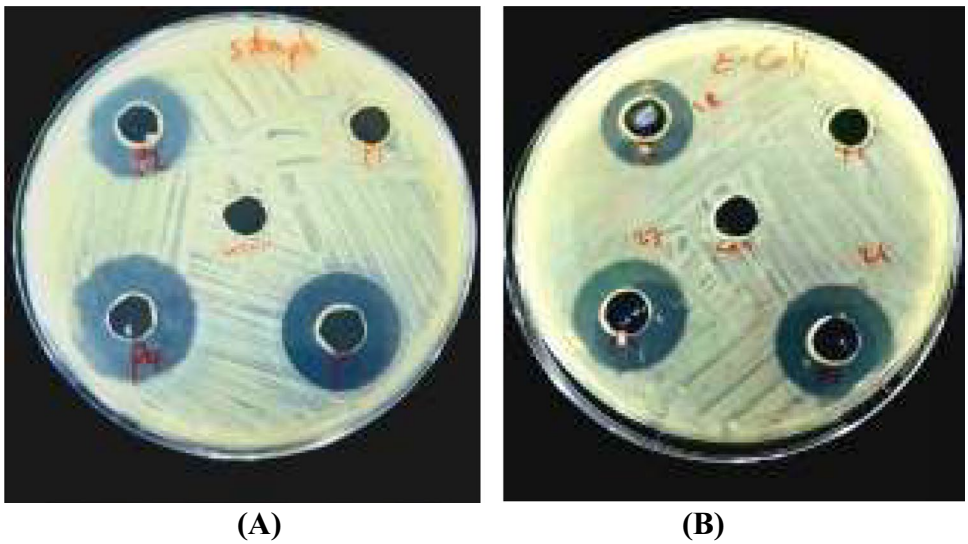

Fig. 19 Image for inhibition zones of (**A**) S. aureus and (**B**) E. coli for samples

frequencies and the migration of charge carriers due to the hopping process are responsible for the rise in AC conductivity. The conductivity improved with increased SiO_2 NPs in the polymer matrix at high frequencies, as presented in Fig. 18B. The electronic polarization and the charge carriers that move by the hopping process also increase, along with AC electrical conductivity. The impact of space fees is to blame for this increase and the formation of a continuous network from SiO_2 inside the (PAAm-PVA-PVP). This behavior is bright for optoelectronics and solar cell devices, in agreement with previous studies [2, 68].

Figure 19 shows the image for inhibition zones of samples against the Escherichia coli (gram-negative) and Staphylococcus aureus (gram-positive) bacteria. The BP1 revealed negative resistance and no killing bacteria for both bicriteria. This finding agrees with other researchers proved of these polymers, where PAAm exhibited a lack of biological activity [15]. Interestingly, the contribution of 1 wt. % of

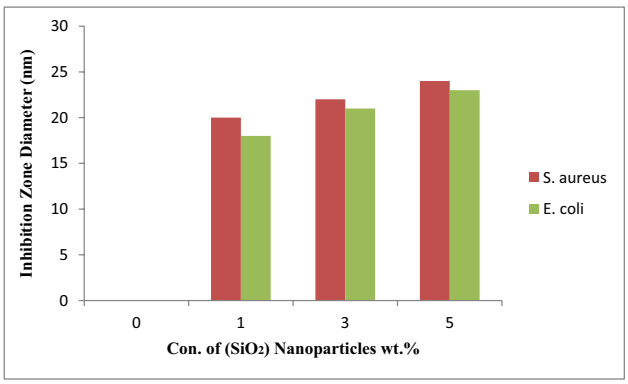

Fig. 20 Antibacterial inhibition zones of S. aureus E. and coli. for samples as a function of SiO_2 nanoparticle concentrations

nanoparticles with the same polymer consecrations of NC1 revealed notable improvements of the antibacterial activity from 00 to 20 and 18 mm, respectively, compared to BP1.

Meanwhile, increasing the SiO_2 loading to 5 wt. % revealed significant improving the inhibition zone up to 24 and 23 mm, respectively, as shown in Fig. 20. Nanoparticles form reactive oxygen species (ROS) and cause the bactericidal action of nanostructures. The electromagnetic interaction could present between the nanoparticles in nanocomposites with the bacteria causes the germs to oxidize and die instantly since the nanocomposites contain positive charges, while the microbes have negative charges. Singlet oxygen (O_2) may be the culprit for destroying the DNA and proteins of bacteria, and ROS, which includes radicals like superoxide radicals, Hydrogen peroxide with hydroxyl radicals (OH) (O-2) (H_2O_2), is the primary mechanism of nanocomposites that is causing the antibacterial activity by using the nanoparticles [63, 69, 70].

4 Conclusions

The following procedure successfully fabricated new nanocomposites using ternary blend polymers PAAm-PVA-PVP reinforced by SiO_2 NPs. The FTIR and XRD present strong interfacial interactions. OM and FESEM images showed a homogeneous surface, and cracks were significantly reduced in the surface with increasing the nanoparticle concentrations. The optical properties of nanocomposite improved with increasing the concentration of SiO_2. The absorbance increases, and the energy gap improves with increases in the concentration of SiO_2 nanoparticles. The dielectric constant and the dielectric loss for nanocomposites were reduced, whereas AC electrical conductivity increases for nanocomposites with the increase in the SiO_2 contained in the matrix. Antibacterial activity for nanocomposites showed enhancement in the inhibition zone value of S. aureus and E. coli with an increasing concentration of SiO_2 nanoparticles which may be used for antibacterial application. The optical and electrical results revealed promising nanocomposites for optoelectronic and solar cell applications.

Acknowledgements The authors would like to thank the department of Physics, University of Babylon, Iraq, for their support.

Authors' Contributions Ehssan Al-Bermany designed the idea and experimental part and performed with analysis of the FTIR, SEM, OMI, and optical properties. Athar Iqbal Alawi performed and wrote the experiments, contributing to the electrical properties and antibacterial activity. Athar Iqbal Alawi wrote the first draft of the paper, and Ehssan Al-Bermany improved, revising the final version. Both authors read and approved the final manuscript.

Data Availability The data are available in the manuscript.

Declarations

Competing Interests The authors declare no competing interests.

Ethics Declarations Not applicable.

Consent to Participate Not applicable.

Consent for Publication Not applicable.

Conflict of Interest The authors declare that they have no conflict of interest.

References

1. Ali Al-Asbahi B, Qaid SMH, Ghaithan HM, Alhamedi Alanezi A (2021) Influence of SiO2/TiO2 nanocomposites on dual resonance Förster energy transfer in ternary hybrid thin films. Results Phys 24:104142. https://doi.org/10.1016/j.rinp.2021.104142
2. Wang Y, Chen J, Do Kim H et al (2018) Ternary blend solar cells based on a conjugated polymer with diketopyrrolopyrrole and carbazole units. Front Energy Res 6:1–9. https://doi.org/10.3389/fenrg.2018.00113
3. Lu L, Chen W, Xu T, Yu L (2015) High-performance ternary blend polymer solar cells involving both energy transfer and hole relay processes. Nat Commun 6:1–7. https://doi.org/10.1038/ncomms8327
4. Pacchioni G, Skuja L, Griscom DL (2012) Defects in SiO2 and related dielectrics: science and technology. In: Pacchioni G, Skuja L, Griscom DL (eds) NATO Science Series II: Mathematics, Physics and Chemistry, NAII, vol 2. Springer Dordrecht. https://doi.org/10.1007/978-94-010-0944-7
5. Wan Z, Huang S, Green MA, Conibeer G (2011) Rapid thermal annealing and crystallization mechanisms study of silicon nanocrystal in silicon carbide matrix. Nanoscale Res Lett 6:1–7
6. Grayson M (1983) Encyclopedia of composite materials and components. Compos Struct 5(1):79–20. https://doi.org/10.1016/0263-8223(86)90015-2
7. Al-Bermany E, Mekhalif AT, Banimuslem HA et al (2023) Effect of green synthesis bimetallic Ag@SiO2 core–shell nanoparticles on absorption behavior and electrical properties of PVA-PEO nanocomposites for optoelectronic applications. Silicon. https://doi.org/10.1007/s12633-023-02332-7
8. Choudhary S (2018) Characterization of amorphous silica nanofiller effect on the structural, morphological, optical, thermal, dielectric and electrical properties of PVA–PVP blend based polymer nanocomposites for their flexible nanodielectric applications. J Mater Sci Mater Electron 29:10517–10534
9. Aldulaimi NR, Al-Bermany E (2022) Tuning the Bandgap and Absorption Behaviour of the Newly-Fabricated Ultrahigh Molecular weight Polyethylene Oxide- Polyvinyl Alcohol/ Graphene Oxide Hybrid Nanocomposites. Polym Polym Compos 30:1–13. https://doi.org/10.1177/09673911221112196
10. Tanaka T, Vaughan AS (2022) Tailoring of nanocomposite dielectrics : from fundamentals to devices and applications. 441. https://doi.org/10.1201/9781315201535
11. Abdali K (2022) Structural, Morphological, and Gamma Ray Shielding (GRS) Characterization of HVCMC/PVP/PEG Polymer Blend Encapsulated with Silicon Dioxide Nanoparticles. Silicon 1–6. https://doi.org/10.1007/s12633-022-01678-8
12. Ghazi RA, Al-Mayalee KH, Al-Bermany E et al (2022) Impact of polymer molecular weights and graphene nanosheets on fabricated PVA-PEG/GO nanocomposites: Morphology, sorption behavior and shielding application. AIMS Mater Sci 9:584–603. https://doi.org/10.3934/matersci.2022035

13. Smith RC, Liang C, Landry M et al (2008) The mechanisms leading to the useful electrical properties of polymer nanodielectrics. IEEE Trans Dielectr Electr Insul 15:187–196. https://doi.org/10.1109/T-DEI.2008.4446750
14. Guo Z, Zhang D, Wei S et al (2010) Effects of iron oxide nanoparticles on polyvinyl alcohol: Interfacial layer and bulk nanocomposites thin film. J Nanopart Res 12:2415–2426. https://doi.org/10.1007/s11051-009-9802-z
15. Luo YL, Chen LL, Xu F, Feng QS (2012) Fabrication and characterization of copper nanoparticles in PVA/PAAm IPNs and swelling of the resulting nanocomposites. Met Mater Int 18:899–908. https://doi.org/10.1007/s12540-012-5024-5
16. Jayaramudu T, Ko H-U, Kim HC et al (2019) Swelling behavior of polyacrylamide–cellulose nanocrystal hydrogels: swelling kinetics, temperature, and pH effects. Materials 12:2080
17. Billmeyer FW (1963) Textbook of Polymer Science. Kobunshi 12:240–251. https://doi.org/10.1295/kobunshi.12.240
18. Kolahalam LA, Kasi Viswanath IV, Diwakar BS et al (2019) Review on nanomaterials: Synthesis and applications. Mater Today Proc 18(6):2182–2190. https://doi.org/10.1016/j.matpr.2019.07.371
19. Ali HE, Atta A, Senna MM (2015) Physico-chemical properties of carboxymethyl cellulose (CMC)/nanosized titanium oxide (TiO2) gamma irradiated composite. Arab J Nucl Sci Appl 48:44–52
20. Hussien HAJ, Kadhim RG, Hashim A (2021) Low-Cost Pressure Sensors Fabricated from Novel Polymeric Nanocomposites. J Phys Conf Ser 1818:012186. https://doi.org/10.1088/1742-6596/1818/1/012186
21. Abdullah OG, Aziz SB, Omer KM, Salih YM (2015) Reducing the optical band gap of polyvinyl alcohol (PVA) based nanocomposite. J Mater Sci Mater Electron 26:5303–5309
22. Abdali K, Rabee BH, Al-Bermany E et al (2023) Effect of Doping Sb2O3 NPs on Morphological, Mechanical, and Dielectric Properties of PVA/PVP Blend Film for Electromechanical Applications. Nano 2350011. https://doi.org/10.1142/S17932920235001 1X
23. Hassan CM, Peppas NA (2000) Structure and Applications of Poly(vinyl alcohol) Hydrogels Produced by Conventional Crosslinking or by Freezing/Thawing Methods. In: Biopolymers PVA Hydrogels, Anionic Polymerisation Nanocomposites. Berlin, Heidelberg: Springer Berlin Heidelberg, pp 37–65
24. NimrodhAnanth A, Umapathy S, Sophia J et al (2011) On the optical and thermal properties of in situ/ex situ reduced Ag NP's/PVA composites and its role as a simple SPR-based protein sensor. Appl Nanosci 1:87–96
25. Gautam A, Ram S (2010) Preparation and thermomechanical properties of Ag-PVA nanocomposite films. Mater Chem Phys 119:266–271. https://doi.org/10.1016/j.matchemphys.2009.08.050
26. Ragab HM, Algethami N, Elamin NY et al (2022) An insight into the influence of Ag/Se nanoparticles on the structural, optical, and electrical properties of Cs/PAM nanocomposites films as application in electrochemical devices. J Mol Struct 1267:133619
27. Gaabour LH (2019) Influence of silica nanoparticles incorporated with chitosan/polyacrylamide polymer nanocomposites. J Market Res 8:2157–2163. https://doi.org/10.1016/j.jmrt.2019.02.003
28. Alsaad AM, Ahmad AA, Dairy ARAL et al (2020) Spectroscopic characterization of optical and thermal properties of (PMMA-PVA) hybrid thin films doped with SiO2 nanoparticles. Results Phys 19:103463. https://doi.org/10.1016/j.rinp.2020.103463
29. Soliman TS, Vshivkov SA, Elkalashy SI (2020) Structural, thermal, and linear optical properties of SiO2 nanoparticles dispersed in polyvinyl alcohol nanocomposite films. Polym Compos 41:3340–3350. https://doi.org/10.1002/pc.25623
30. Mansour AM, Abou Hammad AB, Bakr AM, El Nahrawy AM (2022) Silica Zinc Titanate Wide Bandgap Semiconductor Nanocrystallites: Synthesis and Characterization. Silicon 14:11715–11729. https://doi.org/10.1007/s12633-022-01886-2
31 Jo N-B, Baek J-S, Kim E-S (2021) The Effect of PVA Binder Solvent Composition on the Microstructure and Electrical Properties of 0.98 BaTiO3–0.02 (Ba0. 5Ca0. 5) SiO3 Doped with Dy2O3. Processes 9:2067
32. Abodood AAF, Abdali K, Mousa Al-Ogaili AO et al (2023) Effect of Molar Concentration and Solvent Type on Linear and NLO Properties of Aurintricarboxylic (ATA) Organic Dye for Image Sensor and Optical Limiter Applications. Int J Nanosci. https://doi.org/10.1142/S0219581X2350014X
33. Ali AI, Salim SA, Kamoun EA (2022) Novel glass materials-based (PVA/PVP/Al2O3/SiO2) hybrid composite hydrogel membranes for industrial applications: synthesis, characterization, and physical properties. J Mater Sci: Mater Electron 33:10572–10584. https://doi.org/10.1007/s10854-022-08043-w
34. Omar MA (1975) Elementary solid state physics: principles and applications. Am J Phys 43(10):929–933. https://doi.org/10.1119/1.9980
35. Jothibas M, Manoharan C, Johnson Jeyakumar S, Praveen P (2015) Study on structural and optical behaviors of In2O3 nanocrystals as potential candidate for optoelectronic devices. J Mater Sci Mater Electron 26:9600–9606. https://doi.org/10.1007/s10854-015-3623-x
36. Abdel-Baset T, Elzayat M, Mahrous S (2016) Characterization and optical and dielectric properties of polyvinyl chloride/silica nanocomposites films. Int J Polym Sci 2016:1707018. https://doi.org/10.1155/2016/1707018
37. Agarwal S, Saraswat YK, Saraswat VK (2016) Study of Optical Constants of ZnO Dispersed PC/PMMA Blend Nanocomposites. Open Phys J 3:63–72. https://doi.org/10.2174/1874843001603010063
38. Mahfoudh N, Karoui K, BenRhaiem A (2021) Optical studies and dielectric response of [DMA] 2 MCl 4 (M= Zn and Co) and [DMA] 2 ZnBr 4. RSC Adv 11:24526–24535
39. Alsaad A, Al Dairy AR, Ahmad A et al (2021) Synthesis and Characterization of Polymeric (PMMA-PVA) Hybrid Thin Films Doped with TiO2 Nanoparticles Using Dip-Coating Technique. Crystals 11:99
40. Al-Shawabkeh AF, Elimat ZM, Abushgair KN (2021) Effect of non-annealed and annealed ZnO on the optical properties of PVC/ZnO nanocomposite films. J Thermoplast Compos Mater 36(3):08927057211038631. https://doi.org/10.1177/08927057211038631
41. Haiba AS, Gouda OE, Mahmoud SF, El-gendy AA (2014) Improving the Dielectric Properties of High Density Polyethylene by Incorporating Clay-Nanofiller. TELKOMNIKA (Telecommun Comput Electron Control) 12:763–772
42. South M, Ozonoff S, McMahon WM (2005) Repetitive behavior profiles in Asperger syndrome and high-functioning autism. J Autism Dev Disord 35:145–158
43. Dweik H, Sultan W, Sowwan M, Makharza S (2008) Analysis characterization and some properties of polyacrylamide copper complexes. Int J Polym Mater Polym Biomater 57:228–244. https://doi.org/10.1080/00914030701413280
44. Mansur HS, Sadahira CM, Souza AN, Mansur AAP (2008) FTIR spectroscopy characterization of poly (vinyl alcohol) hydrogel with different hydrolysis degree and chemically crosslinked with glutaraldehyde. Mater Sci Eng C 28:539–548
45. Hendrawan H, Khoerunnisa F, Sonjaya Y, Putri AD (2019) Poly (vinyl alcohol)/glutaraldehyde/Premna oblongifolia merr extract hydrogel for controlled-release and water absorption application. In: IOP Conference Series: Materials Science and Engineering. IOP Publishing, p 12048
46. Abdali K, Al E, Khalid B, Abass H (2023) Impact the silver nanoparticles on properties of new fabricated polyvinyl alcohol

- polyacrylamide - polyacrylic acid nanocomposites films for opto-electronics and radiation pollution applications. J Polym Res 30. https://doi.org/10.1007/s10965-023-03514-y
47. Rao BS, Muralidhar J, Kumar RJ et al (2011) A comparison in radiative degradation of acrylamide polymers. Int J Chem Sci 9:109–116
48. Al Mogbel MS, Elabbasy MT, Mohamed RS et al (2021) Improvement in antibacterial activity of Poly Vinyl Pyrrolidone/Chitosan incorporated by graphene oxide NPs via laser ablation. J Polym Res 28:1–8
49. Al-shammari AK, Al-Bermany E (2022) Polymer functional group impact on the thermo-mechanical properties of polyacrylic acid, polyacrylic amide- poly (vinyl alcohol) nanocomposites reinforced by graphene oxide nanosheets. J Polym Res 29:351. https://doi.org/10.1007/s10965-022-03210-3
50. Aldulaimi NR, Al-Bermany E (2021) New Fabricated UHM-WPEO-PVA Hybrid Nanocomposites Reinforced by GO Nanosheets: Structure and DC Electrical Behaviour. J Phys Conf Ser 1973:012164. https://doi.org/10.1088/1742-6596/1973/1/012164
51. Abdali K (2022) Synthesis, characterization and USW sensor of PEO/PMMA/PVP doped with zirconium dioxide nanoparticles. Trans Electr Electron Mater 23:563–568. https://doi.org/10.1007/s42341-022-00388-7
52. Al-shammari AK, Al-Bermany E (2021) New Fabricated (PAA-PVA/GO) and (PAAm-PVA/GO) Nanocomposites: Functional Groups and Graphene Nanosheets effect on the Morphology and Mechanical Properties. J Phys Conf Ser 1973:012165. https://doi.org/10.1088/1742-6596/1973/1/012165
53. Rajesh K, Crasta V, Rithin Kumar NB et al (2019) Structural, optical, mechanical and dielectric properties of titanium dioxide doped PVA/PVP nanocomposite. J Polym Res 26. https://doi.org/10.1007/s10965-019-1762-0
54. Kadhim MA, Al-Bermany E (2021) New fabricated PMMA-PVA/graphene oxide nanocomposites: Structure, optical properties and application. J Compos Mater 55:2793–2806. https://doi.org/10.1177/0021998321995912
55. MAQ B, Rahman MS (2015) Improvement of Swelling Behaviour of Poly (Vinyl Pyrrolidone) and Acrylic Acid Blend Hydrogel Prepared By the Application of Gamma Radiation. Org Chem Curr Res 04. https://doi.org/10.4172/2161-0401.1000138
56. Desplentere F, Lomov SV, Woerdeman DL et al (2005) Micro-CT characterization of variability in 3D textile architecture. Compos Sci Technol 65:1920–1930
57. Qiu M, Zhang Y, Wen B (2018) Facile synthesis of polyaniline nanostructures with effective electromagnetic interference shielding performance. J Mater Sci Mater Electron 29:10437–10444. https://doi.org/10.1007/s10854-018-9100-6
58. Feng Y, Zhang X, Shen Y et al (2012) A mechanically strong, flexible and conductive film based on bacterial cellulose/graphene nanocomposite. Carbohyd Polym 87:644–649. https://doi.org/10.1016/j.carbpol.2011.08.039
59. Al-Jamal AN, KA O, Abbass KH et al (2023) Silver NPs reinforced the structural and mechanical properties of PVA-PAAm-PEG nanocomposites. AIP Conf Proc 030005:030005. https://doi.org/10.1063/5.0114621
60. Phukan P, Saikia D (2013) Optical and Structural Investigation of CdSe Quantum Dots Dispersed in PVA Matrix and Photovoltaic Applications. Int J Photoenergy 2013:1–6. https://doi.org/10.1155/2013/728280
61. Luo Q, Shan Y, Zuo X, Liu J (2018) Anisotropic tough poly(vinyl alcohol)/graphene oxide nanocomposite hydrogels for potential biomedical applications. RSC Adv 8:13284–13291
62. Fortunati E, Luzi F, Puglia D et al (2015) Processing of PLA nanocomposites with cellulose nanocrystals extracted from Posidonia oceanica waste: Innovative reuse of coastal plant. Ind Crops Prod 67:439–447. https://doi.org/10.1016/j.indcrop.2015.01.075
63. Abdali K, Abass KH, Al-bermany E et al (2022) Morphological, Optical, ElectricalCharacterizations and Anti-Escherichia coli Bacterial Efficiency (AECBE) of PVA/PAAm/PEO Polymer Blend Doped with Silver NPs. Nano Biomed Eng 14:114–122. https://doi.org/10.5101/nbe.v14i2.p114-122.Abstract
64. Dhatarwal P, Sengwa RJ (2021) Nanofiller controllable optical parameters and improved thermal properties of (PVP/PEO)/Al2O3 and (PVP/PEO)/SiO2 nanocomposites. Optik 233. https://doi.org/10.1016/j.ijleo.2021.166594
65. Jabbar SA, Khalil SM, Abdulridha AR et al (2022) Dielectric, AC Conductivity and Optical Characterizations of (PVA-PEG) Doped SrO Hybrid Nanocomposites.pdf. Key Eng Mater 936:83–92. https://doi.org/10.4028/v-3lkwx9
66. Meshram SD, Rupnarayan RV, Jagtap SV et al (2015) Synthesis and characterization of lead oxide nanoparticles. Int J Chem Phys Sci 4:83–88
67. McLachlan DS, Chiteme C, Park C et al (2005) AC and DC percolative conductivity of single wall carbon nanotube polymer composites. J Polym Sci Part B Polym Phys 43:3273–3287
68. Hussein M, Hashim A (2012) Study of Dielectric Properties For (Calcium Oxide-poly-vinyl alcohol) Composites. Basic Education College Magazine For Educational and Humanities Sciences 2012. Acad Sci J 202–207. https://www.iasj.net/iasj/article/75088
69. Prabhu YT, Rao KV, Kumari BS et al (2015) Synthesis of Fe3O4 nanoparticles and its antibacterial application. Int Nano Lett 5:85–92. https://doi.org/10.1007/s40089-015-0141-z
70. Behera SS, Patra JK, Pramanik K et al (2012) Characterization and evaluation of antibacterial activities of chemically synthesized iron oxide nanoparticles. World J Nano Sci Eng 2:196–200. https://doi.org/10.4236/wjnse.2012.24026

Terms and Conditions

Springer Nature journal content, brought to you courtesy of Springer Nature Customer Service Center GmbH (“Springer Nature”).
Springer Nature supports a reasonable amount of sharing of research papers by authors, subscribers and authorised users (“Users”), for small-scale personal, non-commercial use provided that all copyright, trade and service marks and other proprietary notices are maintained. By accessing, sharing, receiving or otherwise using the Springer Nature journal content you agree to these terms of use (“Terms”). For these purposes, Springer Nature considers academic use (by researchers and students) to be non-commercial.
These Terms are supplementary and will apply in addition to any applicable website terms and conditions, a relevant site licence or a personal subscription. These Terms will prevail over any conflict or ambiguity with regards to the relevant terms, a site licence or a personal subscription (to the extent of the conflict or ambiguity only). For Creative Commons-licensed articles, the terms of the Creative Commons license used will apply.
We collect and use personal data to provide access to the Springer Nature journal content. We may also use these personal data internally within ResearchGate and Springer Nature and as agreed share it, in an anonymised way, for purposes of tracking, analysis and reporting. We will not otherwise disclose your personal data outside the ResearchGate or the Springer Nature group of companies unless we have your permission as detailed in the Privacy Policy.
While Users may use the Springer Nature journal content for small scale, personal non-commercial use, it is important to note that Users may not:

1. use such content for the purpose of providing other users with access on a regular or large scale basis or as a means to circumvent access control;
2. use such content where to do so would be considered a criminal or statutory offence in any jurisdiction, or gives rise to civil liability, or is otherwise unlawful;
3. falsely or misleadingly imply or suggest endorsement, approval , sponsorship, or association unless explicitly agreed to by Springer Nature in writing;
4. use bots or other automated methods to access the content or redirect messages
5. override any security feature or exclusionary protocol; or
6. share the content in order to create substitute for Springer Nature products or services or a systematic database of Springer Nature journal content.

In line with the restriction against commercial use, Springer Nature does not permit the creation of a product or service that creates revenue, royalties, rent or income from our content or its inclusion as part of a paid for service or for other commercial gain. Springer Nature journal content cannot be used for inter-library loans and librarians may not upload Springer Nature journal content on a large scale into their, or any other, institutional repository.
These terms of use are reviewed regularly and may be amended at any time. Springer Nature is not obligated to publish any information or content on this website and may remove it or features or functionality at our sole discretion, at any time with or without notice. Springer Nature may revoke this licence to you at any time and remove access to any copies of the Springer Nature journal content which have been saved.
To the fullest extent permitted by law, Springer Nature makes no warranties, representations or guarantees to Users, either express or implied with respect to the Springer nature journal content and all parties disclaim and waive any implied warranties or warranties imposed by law, including merchantability or fitness for any particular purpose.
Please note that these rights do not automatically extend to content, data or other material published by Springer Nature that may be licensed from third parties.
If you would like to use or distribute our Springer Nature journal content to a wider audience or on a regular basis or in any other manner not expressly permitted by these Terms, please contact Springer Nature at

onlineservice@springernature.com